2008 Annual SCEC report

InSAR velocity maps of Southern California from ERS and ENVISAT data (PI: Fialko)

Publications and abstracts resulted from this project:

Wei, M., D. Sandwell and Y. Fialko, A Silent M4.8 slip event of October 3-6, 2006, on the Superstition Hills fault, Southern California, J. Geophys. Res. (in press).

Fialko, Y. and D. Rivet, Secular and Transient Deformation in the Eastern California Shear Zone from InSAR and GPS Observations Over 1992-2007 Epoch, Eos, Trans. AGU, 89(23), Suppl., abst. G33B-01 (Invited), 2008.

Fialko, Y., M. Manzo, F. Casu, A. Pepe, R. Lanari, Time Series of Deformation in Southern California From 15 Years of InSAR Observations, Eos, Trans. AGU, 89(53), Suppl., abst. G23A-06, 2008.

Barbot, S. and Y. Fialko, Estimation of Relative Contributions of Localized Shear vs Broad Viscous Flow in Postseismic Transients: Case Study of the 1992 Landers and 1999 Hector Mine, California, Earthquakes, Eos, Trans. AGU, 89(53), Suppl., abst. T53C-1969, 2008.

Summary of results:

Development of efficient algorithms for processing of large volumes of InSAR data

As the main limitation to the InSAR measurements of small-amplitude ground velocities associated with interseismic deformation (centimeters per year or less) is the atmospheric noise (*Goldstein*, 1995; *Tarayre and Massonnet*, 1996; *Zebker et al.*, 1997), we are taking advantage of redundancy of SAR acquisitions to improve the signal-to-noise ratio. Toward this end, we have developed new algorithms for stacking of multiple interferograms and recovery of timeseries of the LOS displacements, which can effectively push InSAR technique toward accuracy for the line of sight (LOS) velocities of order of 10^{-3} m/yr (e.g., *Berardino et al.*, 2002; *Fialko and Simons*, 2001; *Peltzer et al.*, 2001). Our method makes use of the fact that the phase contribution due to atmosphere changes sign in "consecutive" interferograms that share a common acquisition. By quantifying the magnitude of the sign-flipping phase we can identify SAR acquisitions that are highly affected by the atmospheric noise, and construct an optimal "stacking tree" that minimizes the contribution of such noisy scenes. The scheme entails the following steps:

1. Generate a set of interferograms for a prescribed range of perpendicular baselines and time spans.
2. Select a subset of interferograms with sufficient correlation and coverage.
3. Evaluate Atmospheric Noise Coefficients (ANC) for each SAR acquisition. We do so by subdividing the interferometric "connectivity tree" into triplets, and computing some norm of range changes for every interferogram, as well as for sums of sequential interferograms sharing a common scene. We identify these coefficients for all shared SAR scenes in a data set.
4. Finally, we minimize the contribution of SAR acquisitions that were deemed noisy by re-arranging the "connectivity tree" around such acquisitions so that the number of "in-coming" and "outgoing" connections is the same (Figure 1). Thus the contribution of noisy scenes is canceled out: interferograms involving noisy scenes are used in the stack, but such scenes do not affect the stacked radar phase. The degree of suppression (the difference between the in-coming and outgoing connections) of a particular scene may be adjusted depending on the magnitude of ANC. Note that interferometric pairs affected by significant non-steady deformation - e.g., due to an earthquake - may be used for stacking upon subtracting the coseismic signal (using either a model

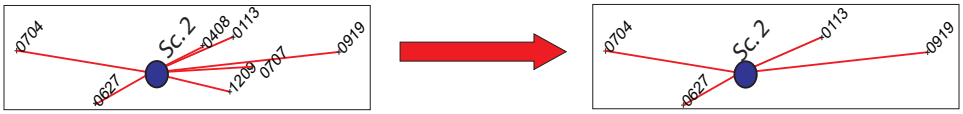

Figure 1: Partial elimination of interferograms that cancels a contribution of a "noisy" SAR scene.

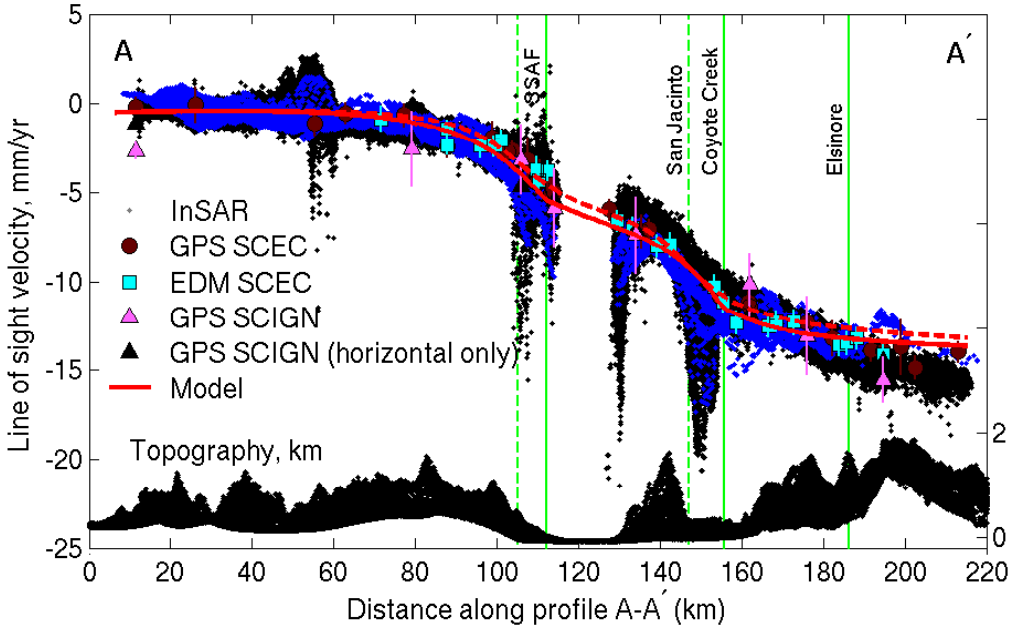

Figure 2: LOS velocities from a profile across the southern SAF (*Fialko*, 2006) over a time interval 1992-2006, as inferred from the SBAS time series analysis (black dots) and ANR method (blue dots).

or shorter-term coseismic interferograms).

We have performed a comprehensive evaluation of the described algorithm by comparing results with those obtained using other techniques, as well as independent data, such as continuous GPS. In particular, we compared the mean velocity field computed using the ANR method to that obtained using the Small Baseline Subset (SBAS) method (*Berardino et al.*, 2002; *Casu et al.*, 2006). To perform this cross-validation, we collaborated with the InSAR research group at IREA, Italy. SBAS method computes time series of LOS displacements for every coherent pixel in a given set of interferograms. These time series can be then interpolated on a pixel by pixel basis to obtain a mean velocity map. Figure 2 shows LOS velocities across the southern San Andreas Fault (track 356, see *Fialko* (2006)) inferred using the two techniques. Velocities obtained using the two approaches are essentially identical. Results shown in Figure 2 lend support to our previous estimates of the LOS velocity field across the Coachella Valley segment of the SAF (*Fialko*, 2006). The data show a clear pattern of elastic strain accumulation on both faults (including the Anza Gap on the San Jacinto fault). LOS velocities from stable pixels in otherwise uncorrelated areas confirm significant subsidence in the Coachella Valley (*Fialko*, 2006), and help define the diffuse plate boundary around the Brawley seismic zone. The observed strain patterns can be readily interpreted in terms of present-day slip rates using numerical models of interseismic deformation (2009 SCEC proposal, work in progress).

Development of efficient algorithms for processing of large volumes of InSAR data

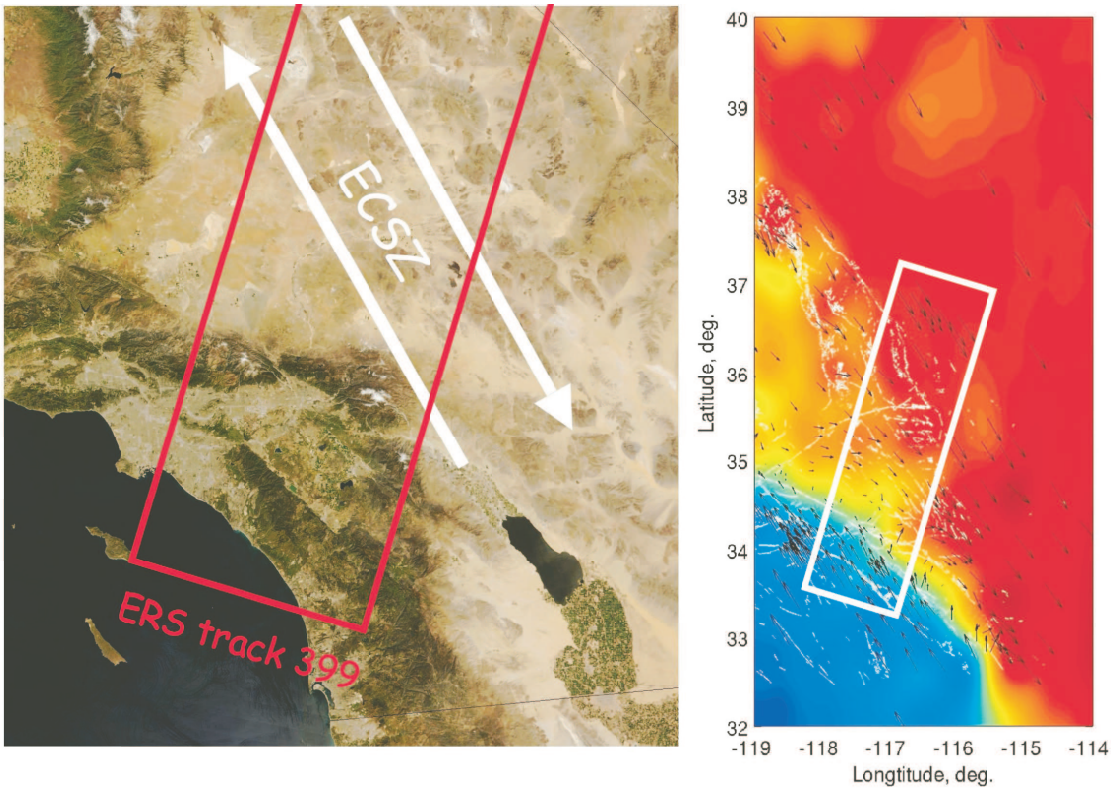

Figure 3: (Left) Landsat image of Southern California indicating the radar swath (red rectangle) and the location and sense of shear of the Eastern California Shear Zone (ECSZ). (Right) Color indicates predicted variations in the satellite LOS velocity, based on interpolation of continuous GPS data (see black arrows). Quaternary faults are shown by white curvy lines, and white rectangle denotes the position of the radar swath, as in the left panel.

We have applied the developed methodology to a dense catalog of ERS-1, ERS-2, and ENVISAT data from the descening track 399 that crosses the Eastern California Shear Zone, the Mojave segment of the San Andreas fault, and epicentral areas of two largest earthquakes in Southern California in 20 years: the M7.3 Landers and M7.1 Hector Mine earthquakes. Figure 3 shows the extent of the radar swath, as well as the predicted variations in the ground velocity along the satellite line-of-sight (LOS), based on interpolation of continuous GPS data. Figure 4 shows inferred LOS velocity fields from track 399 over two subsequent 7-year epochs, including post-seismic contributions from the Landers (1992-1999) and Hector Mine (2000-2007) earthquakes. The stacked InSAR data reveal several features that were not apparent in any individual interferogram. There are a number of lineated zones of high gradients in the LOS velocities that are correlated with the geologically mapped faults.

Another particular area of interest is the rate and style of deformation across the Blackwater fault ($\sim$ 117.3°W, 35.3°N). Previous InSAR studies using data from the ERS track 170 have suggested that this fault may undergo an accelerated transient deformation following the 1992 Landers earthquake (*Peltzer et al.*, 2001). Here we demonstrate how independent data from nearby overlapping tracks can be used to limit uncertainties in our interpretation of the LOS data Figure 5 shows the satellite range changes from a profile A-A$'$ across the Blackwater fault from the descending track 399 (that partially overlaps track 170 from the east), and ascending track 349. To test the signal consistency along the fault, and further increase the signal-to-noise ratio, we collapse all

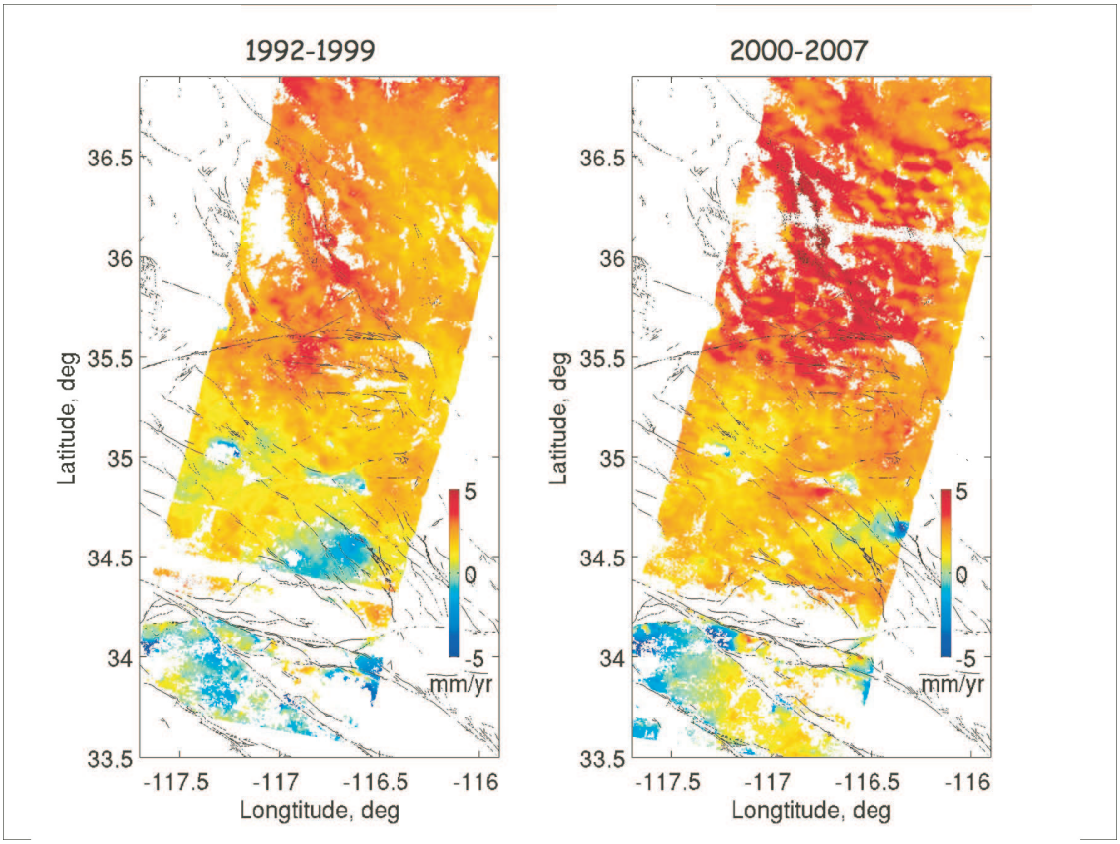

Figure 4: Interferometric stacks from the descending satellite track 399 over two 7-year epochs (approximately, before and after the Hector Mine earthquake). Colors denote the average LOS velocities (stacked LOS displacements divided by the total time span of all interferograms in the stack), in cm/yr (positive toward the satellite). Black wavy lines denote Quaternary faults (*Jennings*, 1994).

the data points within 10 km of the profile onto the line A-A′. Our results from the descending track 399 indicate high gradients in the LOS velocity across the Blackwater fault over a time period 1992-1999 (Figures 4 and 5), in agreement with *Peltzer et al.* (2001) findings, which essentially rules out atmospheric artifacts. If the observed LOS velocity variations across the fault are interpreted as indicating a predominantly horizontal motion due to the interseismic fault creep at depth, the localized nature of the LOS displacements requires an abnormally small depth to the brittle-ductile transition of the order of 3 km (Figure 5).

Analysis of *Peltzer et al.* (2001) yielded a similar value of the fault locking depth of 5 km. Data from the ascending track 349 indicate that a substantial fraction of the observed strain anomaly may be in fact due to differential vertical motion, such that the western side of the fault subsides with respect to the eastern side. This follows from different sensitivities of the LOS displacements from different viewing geometries: if the signal were predominantly due to right-lateral strain, range changes from the ascending orbit should be smaller in magnitude, and of opposite sign compared to those from the descending orbit. A predominantly vertical deformation would result in comparable signals in interferometric stacks from the ascending and descending orbits, as observed (Figure 5). The same analysis revealed much smaller (if any) deformation across the Blackwater fault over the 2000-2007 epoch, implying a transient nature of the observed strain, possibly related to the 1992 Lander earthquake (*Peltzer et al.*, 2001). Our preferred interpretation is that the localized vertical

strain on the Blackwater fault is due to a predominantly elastic deformation of a compliant fault zone surrounding the primary slip surface. Existence of wide (up to a few kilometers) zones of reduced elastic moduli around several faults in the Eastern California Shear Zone has been inferred from the analysis of InSAR data from the Hector Mine (*Fialko et al.*, 2002) and Landers (*Fialko*, 2004) earthquakes, and recently verified with seismic tomography for the Calico fault (*Cochran et al.*, 2006). According to the compliant fault zone model, the observed strain concentration on the Blackwater fault may represent a secular subsidence of the western side of the fault accommodated across a compliant fault zone that is ∼2-3 km wide. Besides removing the need for an abnormally thin seismogenic layer, this interpretation may reconcile the short-term geodetic and the long-term geologic slip rates (e.g., *Oskin and Iriondo*, 2004).

Analysis of a silent slip event of Oct. 2006 on the Superstition Hills Fault

During October of 2006, the 20-km long Superstition Hills fault (SHF) in the Salton Trough, Southern California, slipped aseismically producing a maximum offset of 27 mm as recorded by a creepmeter (operated by Roger Bilham of Colorado University). We investigated this creep event, as well as the spatial and temporal variations in slip history since 1992 using ERS and ENVISAT satellite data. During a 15-year period, quasi-steady creep was found to be punctuated by at least three events. The first two events were dynamically triggered by the 1992 Landers and 1999 Hector Mine earthquakes. In contrast, there was no obvious triggering mechanism for the October 2006 event. We showed that field measurements of fault offset after the 1999 and 2006 events are in good agreement with the InSAR data. Such an agreement indicates that creep occurred along the 20 km-long fault above 4 km depth with most of the slip occurring at the surface. The moment released during this event is equivalent to a M_w4.7 earthquake. This event produced no detectable aftershocks and was not recorded by the continuous GPS stations that were 9 km away. Modeling of the long-term creep from 1992 to 2007 creep using stacked ERS interferograms also shows a maximum creep depth of 2-4 km with slip tapering with depth. Considering that the sediment thickness varies between 3 km and 5 km along the SHF, our results are consistent with pervious studies suggesting that shallow creep is controlled by sediment depth, possibly due to induced high pore pressures in unconsolidated sediments.

References

Berardino, P., G. Fornaro, R. Lanari, and E. Sansosti, A new algorithm for surface deformation monitoring based on small baseline differential SAR interferograms, *IEEE Trans. Geosci. Rem. Sens.*, *40*, 2375–2383, 2002.

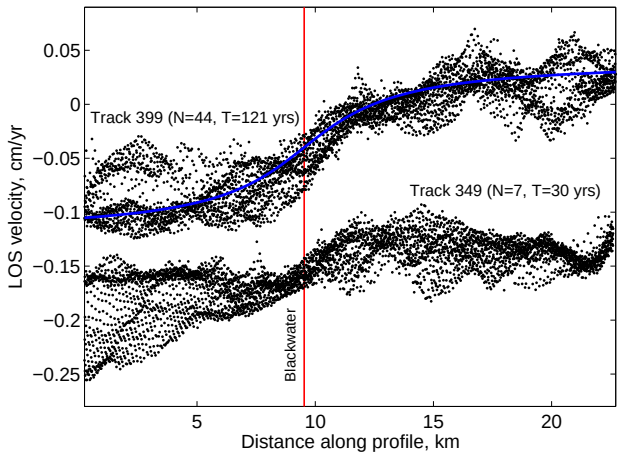

Figure 5: Variations in the satellite LOS velocities across the Blackwater fault. Black dots denote the stacked InSAR data from the 10 km wide swath collapsed onto profile A-A′ from the descending track 399 (top), and the ascending track 349 (bottom). N is a number of interferograms in a stack, and T is their cumulative time span. Red line shows the position of the fault trace. Blue line shows the predicted interseismic velocity assuming the locking depth of 3 km.

Casu, F., M. Manzo, and R. Lanari, A quantitative assessment of the SBAS algorithm performance for surface deformation retrieval from DInSAR data, *Rem. Sens. Env.*, *102*, 195–210, 2006.

Cochran, E. S., M. Radiguet, P. M. Shearer, Y.-G. Li, Y. Fialko, and J. E. Vidale, Seismic Imaging of the Damage Zone Around the Calico Fault, *Eos Trans. AGU*, p. (submitted), 2006.

Fialko, Y., Probing the mechanical properties of seismically active crust with space geodesy: Study of the co-seismic deformation due to the 1992 M_w7.3 Landers (southern California) earthquake, *J. Geophys. Res.*, *109*, B03,307, 10.1029/2003JB002,756, 2004.

Fialko, Y., Interseismic strain accumulation and the earthquake potential on the southern San Andreas fault system, *Nature*, *441*, 968–971, 2006.

Fialko, Y., and M. Simons, Evidence for on-going inflation of the Socorro magma body, New Mexico, from Interferometric Synthetic Aperture Radar imaging, *Geophys. Res. Lett.*, *28*, 3549–3552, 2001.

Fialko, Y., D. Sandwell, D. Agnew, M. Simons, P. Shearer, and B. Minster, Deformation on nearby faults induced by the 1999 Hector Mine earthquake, *Science*, *297*, 1858–1862, 2002.

Goldstein, R. M., Atmospheric limitations to repeat-track radar interferometry, *Geophys. Res. Lett.*, *22*, 2517–2520, 1995.

Jennings, C., *Fault activity map of California and adjacent areas, with locations and ages of recent volcanic eruptions*, California Division of Mines and Geology, Geologic Data Map No. 6, map scale 1:750,000, 1994.

Oskin, M., and A. Iriondo, Large-magnitude transient strain accumulation on the Blackwater fault, Eastern California shear zone, *Geology*, *32*, 313–316, 2004.

Peltzer, G., F. Crampe, S. Hensley, and P. Rosen, Transient strain accumulation and fault interaction in the Eastern California shear zone, *Geology*, *29*, 975–978, 2001.

Tarayre, H., and D. Massonnet, Atmospheric propagation heterogeneities revealed by ERS-1 interferometry, *Geophys. Res. Lett.*, *23*, 989–992, 1996.

Zebker, H. A., P. A. Rosen, and S. Hensley, Atmospheric effects in interferometric synthetic aperture radar surface deformation and topographic maps, *J. Geophys. Res.*, *102*, 7547–7563, 1997.